The 4th International Symposium - Supercritical CO2 Power Cycles
September 9-10, 2014, Pittsburgh, Pennsylvania

DEVELOPMENT OF A DIRECT SUPERCRITICAL CARBON DIOXIDE SOLAR RECEIVER BASED ON COMPACT HEAT EXCHANGER TECHNOLOGY

Saeb M. Besarati
Clean Energy Research Center
Tampa, Florida, United States
sbesarati@mail.usf.edu

D. Yogi Goswami
Clean Energy Research Center
Tampa, Florida, United States
goswami@usf.edu

Elias Stefanakos
Clean Energy Research Center
Tampa, Florida, United States
stefanak@eng.usf.edu

Saeb M. Besarati is a Ph.D. candidate in University of South Florida and works as a research assistant in Clean Energy Research Center. His Ph.D. dissertation is entitled as "Analysis of advanced supercritical carbon dioxide power cycles for concentrated solar power applications." His main research interests are modeling and optimization of energy systems. He has contributed in writing two book chapters and 14 refereed technical papers.

Prof. Yogi Goswami is the Distinguished University Professor, and the Director of the Clean Energy Research Center at the University of South Florida. He is the Editor-in-Chief of the "Solar Energy" journal. Dr. Goswami has published 16 books, 17 book chapters, and more than 300 refereed technical papers, and holds 16 patents. He has served as the President of the International Solar Energy Society (ISES), a Governor of ASME-International, Senior Vice President of ASME and President of the International Association for Solar Energy Education (IASEE). Dr. Goswami is the recipient of more than 50 awards and certificates from major engineering and scientific societies for his work in renewable energy.

Prof. Stefanakos is the director of the Clean Energy Research Center (CERC) and Professor of Electrical Engineering at the University of South Florida located in Tampa, Florida. He has ten patents, has edited two books and published two book chapters and over 150 research papers in refereed journals and international conferences. He is a senior member of Institute of Electrical and Electronics Engineers (IEEE), Editor-in-Chief of the Journal of Power and Energy Engineering, associate editor of the Journal of Solar Energy and co-editor of the Journal of Asian Electric Vehicles.

ABSTRACT

Supercritical carbon dioxide (s-CO_2) has recently been proposed as a heat transfer and a working fluid in concentrated solar power (CSP) plants. However, s-CO_2 power cycles operate at exceedingly high pressures (close to 20 MPa). Design of a high temperature solar receiver that can operate at such high pressures while maintaining a superior thermal performance, is a challenge. In this study, a receiver based on compact heat exchanger (CHE) technology is developed. The receiver consists of a group of plates with square-shape channels which are diffusion bonded together. The receiver is expected to heat s-CO2 from 530℃ to 700℃ for a recompression Brayton cycle under optimized operating conditions. A computational model of

the receiver is developed based on a thermal resistance network model and validated against the available data in the literature. By performing a multi-objective Pareto based optimization, the optimal geometry of the CHE is selected. Then, a $3MW_{th}$ cavity receiver is designed using the CHE receivers as individual panels receiving solar flux from the heliostat field. Convective and radiative heat transfer models are employed to calculate bulk fluid and surface temperatures. Finally, it is shown that the desired temperature for s-CO2 is achieved while the surface temperatures remained below the maximum temperature limit of the materials. The receiver efficiency was obtained as 81.22%, which can be further improved by optimizing the geometry of the cavity.

INTRODUCTION

Carbon dioxide is a highly stable compound with low critical properties, which has been proposed as a heat transfer and a working fluid in the next generation of CSP plants (Turchi 2009). Closed-loop Brayton cycles using carbon dioxide in the supercritical state can achieve more than 50% efficiency at operating conditions that can be met in solar power tower plants (Turchi et al. 2012). Moreover, the efficiency of the cycle can be further improved by including an appropriate bottoming cycle (Besarati & Goswami 2013). The main advantages of the s-CO_2 power cycles can be summarized as high efficiency, high power density, and compactness (Turchi et al. 2012).

On the other hand, carbon dioxide seems like a proper replacement for current heat transfer fluids (HTFs), i.e. oil, molten salt, and steam. The main disadvantages of these HTFs are maximum operating temperature limit, required freeze protection units and complex control systems (Turchi 2009). However, the main challenge of utilizing s-CO_2 as the HTF is to design a receiver which can operate at high operating pressures (about 20 MPa) while maintaining outstanding thermal performance. The existing tubular and windowed receivers are not suitable for this application, and innovative design is required to provide appropriate thermal performance as well as high mechanical strength.

Diffusion bounded compact heat exchangers (CHEs) have been extensively used in industry and are recognized for their high efficiency as well as mechanical strength (Hesselgreaves 2001). According to (Li et al. 2011), plate fin heat exchangers and printed circuit heat exchangers (PCHE) that are diffusion bonded can tolerate pressures as high as 60 MPa. Therefore, diffusion bonded CHEs seem to be perfect candidates for future thermal receivers.

In this paper, a CHE is designed to heat s-CO_2 up to 700℃. Inconel 625 is selected as the base material in view of its superior resistance against corrosion in a s-CO_2 environment (Firouzdor et al. 2013)(Gibbs 2010). The thermal model is developed based on the resistance network model and validated against the data in the literature. The mechanical strength of the CHE is also evaluated by the ASME code for pressure vessels. Afterwards, the optimal geometry of the heat exchanger is found by multi-objective Pareto optimization. Then, a $3MW_{th}$ cavity receiver is designed using the designed CHEs as the surface absorbers. The radiative and convective heat transfer models are employed to find the heat loss and efficiency of the receiver.

COMPUTATIONAL MODEL FOR THE CHE

Heat transfer model

The three-dimensional thermal resistance network model developed by Lei et al. (Lei et al. 2007) (Lei 2006) is employed to find the bulk fluid temperature inside the channels and surface temperature profiles. A detailed description of the model and computational algorithm can be found in (Lei 2006). Figure 1 depicts the geometric parameters as well as the thermal resistance network model. A constant heat flux is applied to the top surface.

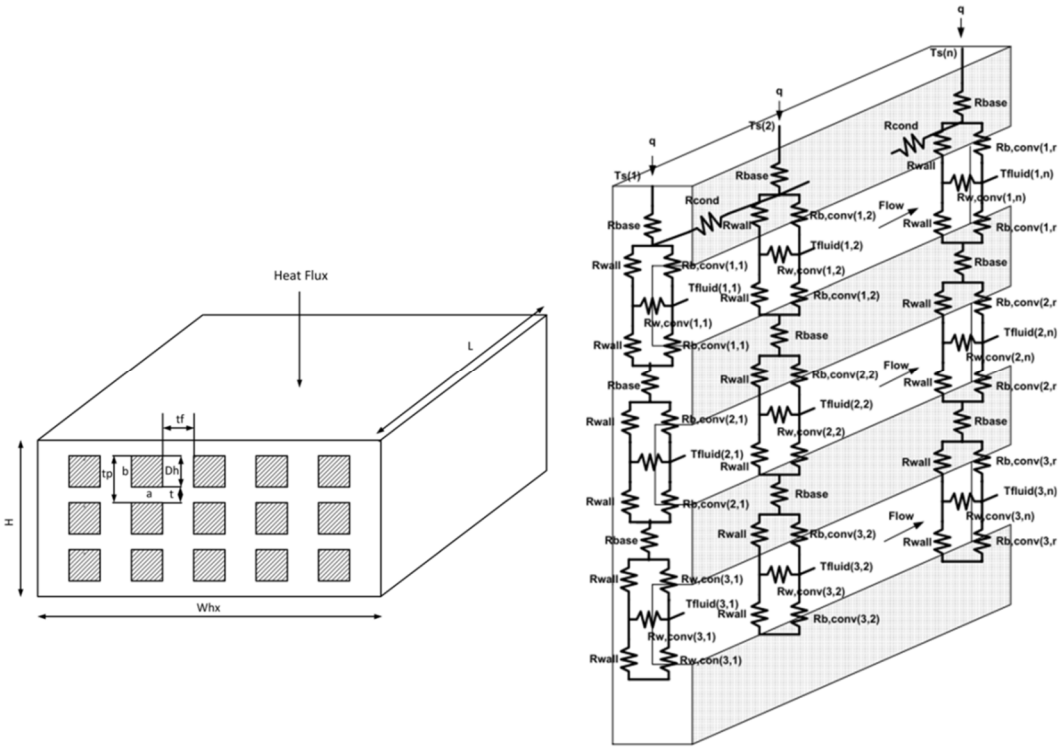

Figure 1. (Left) Geometric configuration; (Right) Thermal resistance network model (Lei 2006).

The channels are divided into n unit grids along the axial direction. The equations for the thermal resistances are given in Table 1. A mesh current analysis is employed to find the heat flux entering each channel. Then, the bulk fluid temperature can be found as:

$$T_{bulk,f}(l,k) = T_{f,in} + \frac{m}{\dot{m} \times C_p} \sum_{i=1}^{k} q(l,i) \quad (1)$$

where l represents the row number, and k is the grid number in the axial direction. The equivalent thermal resistance is given as:

$$R_{eq}(l,k) = \frac{T_j(k) - T_{bulk,f}(l,k)}{q(l,k)} \quad (2)$$

Writing the energy balance around grid k leads to:

$$-T_j(k-1) + \left[2 + R_{cond} \sum_{l=1}^{m} \frac{1}{R_{eq}(l,k)}\right] T_j(k) - T_j(k+1) = R_{cond} \left[q + \sum_{l=1}^{m} \frac{T_{bulk,f}(l,k)}{R_{eq}(l,k)}\right] \quad (3)$$

Therefore, a system of linear equations is obtained for n unknown junction temperatures. These equations are solved by enforcing boundary conditions and using an iterative calculation method.

For the laminar flow (Re<2300), the Nusselt number is calculated by (Hesselgreaves 2001):

$$Nu = 8.235\,(1 - 2.0421\alpha + 3.0853\alpha^2 - 2.4765\alpha^3 + 1.0578\alpha^4 - 0.1861\alpha^5) \quad (4)$$

where α is the aspect ratio.

Table 1. Equations for thermal resistances

Thermal resistance $(\frac{\mathrm{K}}{\mathrm{W}})$	Equation
R_{base}	$\frac{t}{k_s \times \frac{1}{2}(t_f + a) \times l_n}$ (5)
R_{wall}	$\frac{b}{k_s \times t_f \times l_n}$ (6)
R_{cond}	$\frac{l_n}{k_s\left((t_f + a) \times H - m \times a \times b\right)}$ (7)
$R_{w,conv}$	$\frac{1}{h \times b \times l_n}$ (8)
$R_{b,conv}$	$\frac{2}{h \times a \times l_n}$ (9)

Gnielinski correlation (Gnielinski 1976) is used for the turbulent region ($Re > 5000$):

$$Nu = \frac{\frac{f_c}{8}(Re - 1000)Pr}{1 + 12.7\,(Pr^{2/3} - 1)\sqrt{\frac{f_c}{8}}} \quad (10)$$

where Pr is the Prandtl number and f_c is given as:

$$f_c = \left(\frac{1}{1.8\log Re - 1.5}\right)^2 \quad (11)$$

Linear interpolation is used to find the Nusselt number in the transient region.

Pressure drop model

The entrance and exit pressure drops can be estimated by:

$$\Delta P = C\,\rho\frac{V^2}{2}\,/1000 \quad (12)$$

Where C is the loss coefficient, which is assumed 0.5 for the entrance and 1.0 for the exit (Dostal 2004).

The pressure drop inside the channels is calculated by:

$$\Delta P = (f\frac{L}{D_h}\rho\frac{V^2}{2})/1000 \quad (13)$$

The friction factor correlations are provided by (Idelchik 1994) for an extensive range of Reynolds number and relative roughness. In this paper, the surface roughness is $10^{-5}\mathrm{m}$ in all calculations. The overall pressure drop is the average of the pressure drop in all the channels. Refprop (Lemmon et al. 2013) is used to estimate the fluid properties inside the channels.

Model validation

The model is validated against the data given by (Lei 2006). Figure 2 compares the top surface temperature of a CHE for different volumetric flow rates of water. SiC is the base material, and a uniform heat flux density of 2 Watts is applied to the top surface. This is equivalent to a flux density of about 111 $\mathrm{kW/m^2}$. As can be clearly seen, the model predicts the surface temperatures accurately and can be confidently used. The results given by Lei were already validated against the experimental data (Lei 2006).

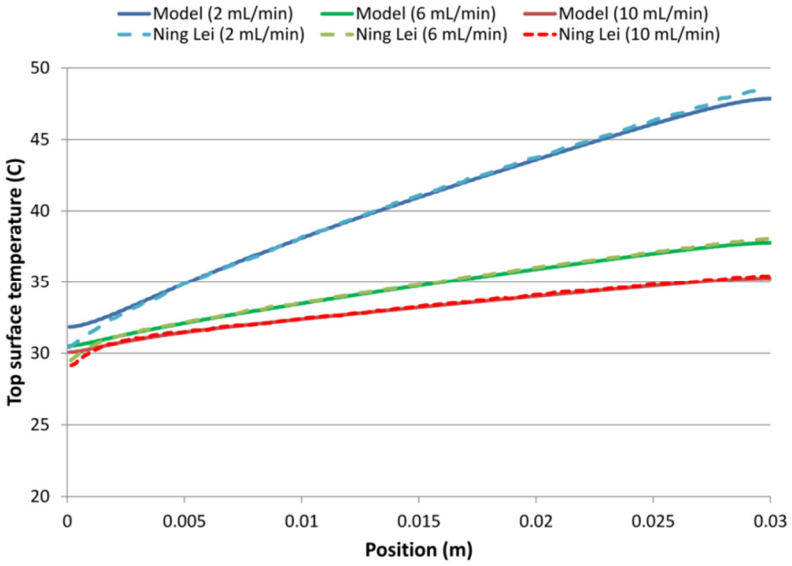

Figure 2. Model validation against the data given by (Lei 2006)

GEOMETRIC OPTIMIZATION OF THE CHE

The unit thermal resistance and pressure drop are considered as the objective functions that need to be minimized simultaneously. The unit thermal resistance is defined as (Lei 2006):

$$RR = \left(\frac{\overline{T_s} - T_{f,in}}{q^{"}}\right) \times 10000 \quad (14)$$

where $\overline{T_s}$ is the mean surface temperature. The hydraulic diameter of the square-shaped channels, number of layers, i.e. number of channels in the vertical direction, and distance between the channels in a single layer are the design variables that need to be determined using multi-objective Pareto optimization. Mechanical strength of the CHE is the constraint, which is evaluated using the ASME boiler and pressure vessel code (Anon 1998). It is essential to maintain:

$$S_m < S \times E \quad (15)$$

and

$$S_T < 1.5 \times S \times E \quad (16)$$

where S_m is the membrane stress, S is the design stress, S_T is the total stress, and E is the joint factor which is given as 0.7 for the diffusion bonded blocks (Pierres et al. 2011). The detailed equations for calculating the membrane and total stresses can be found in (Pierres et al. 2011) and (Anon 1998). The design stress for Inconel 625 is 107 ksi (Everhart 1971).

A uniform heat flux density of 500 $\frac{\mathrm{kW}}{\mathrm{m^2}}$ is applied to the top surface. The fluid inlet temperature to the receiver is 530℃, which is obtained by optimizing the performance of a recompression

Brayton cycle for an ambient temperature of 35℃, turbine inlet temperature of 700℃, and turbine inlet pressure of 20MPa. The mass flow rate is 1 kg/s. The width of the CHE is fixed at 600 mm, the plate thickness is set at 3 mm and the side margin thickness, i.e. the distance between the side wall and the first channel, is 5 mm. During the optimization process, the length of the CHE is fixed at 500 mm.The range of variations in hydraulic diameter, number of layers and distance between the channels are 0.5-3 mm, 3-10, and 1-5 mm, respectively. The number of layers, m, has to be an integer number. A non-dominated sorting genetic algorithm II (NSGA-II) (Deb et al. 2002) is employed for the optimization.

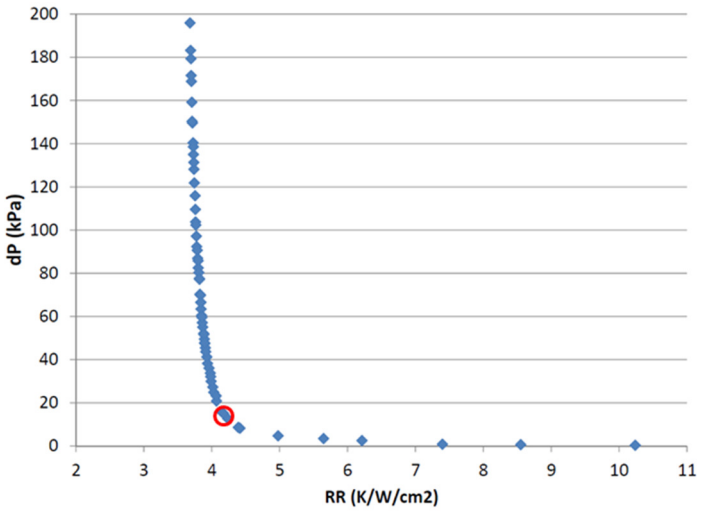

Figure 3. Pareto front of the pressure drop and the unit thermal resistance.

Figure 3 depicts the Pareto front of the objective functions which are in conflict with each other. The point shown with a red circle is considered as an appropriate design condition for the CHE. At this point D_h, m, and t_f are given as 2.8 mm, 3 mm, and 5 mm, respectively. The length of the CHE is then updated until the average bulk fluid temperature at the outlet of the receiver reaches 700℃. The required length of the CHE is obtained as 750 mm accordingly.

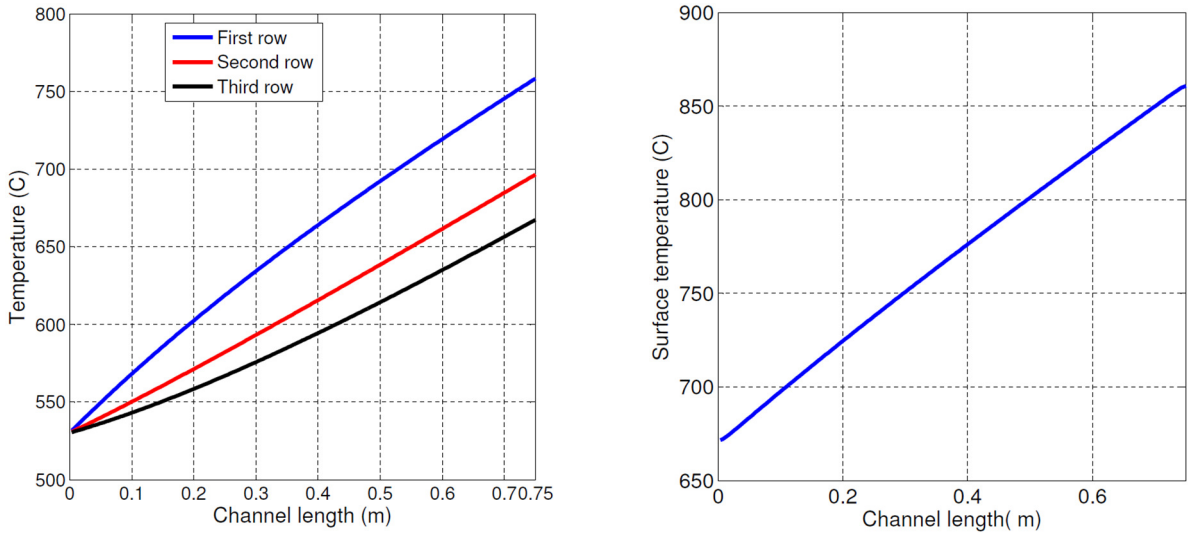

Figure 4. (Left) Temperature profiles of s-CO_2 inside the optimized CHE; (Right) Temperature profile of the surface receiving heat flux

Figure 4 shows the bulk fluid temperature in three layers of the optimized CHE and the temperature profile of the top surface, where the heat flux is applied. As can be clearly seen, the mean bulk fluid temperature at the outlet of the CHE is 700℃ while the maximum surface temperature is 861℃, which is well below the maximum temperature limit of Inconel 625, i.e. 982℃.

CAVITY RECEIVER

A 3 MW_{th} cavity receiver is designed using the optimized CHEs as the surface absorbers. There are 14 panels which are located at the back side of the cavity. Optimization of the cavity geometry is not considered in this study. Figure 5 depicts the schematic of the cavity receiver as well as the geometries of the heat absorbing panels.

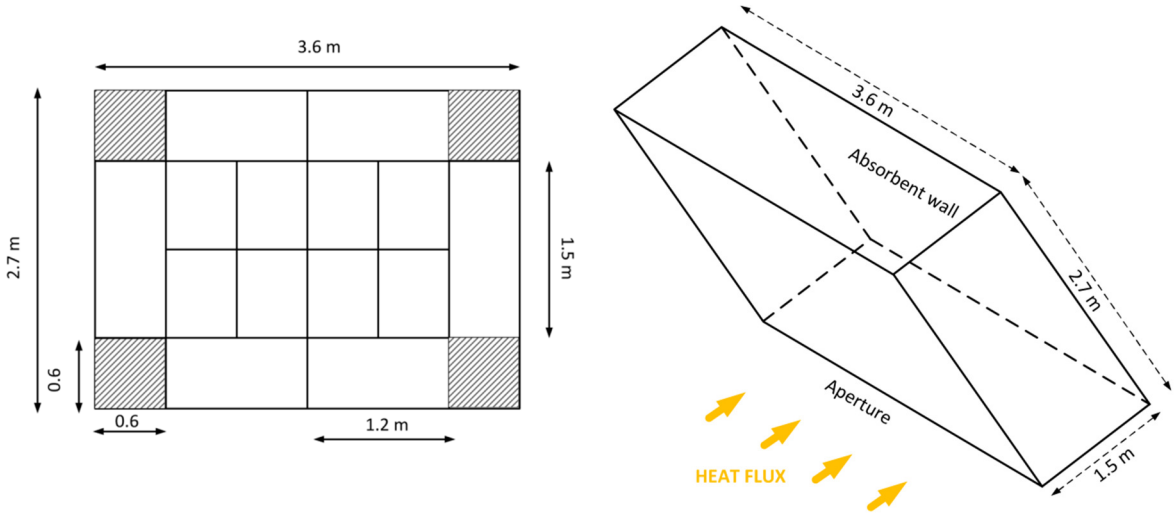

Figure 5. (Left) Heat absorbing panels; (Right) Cavity Receiver

As can be seen, the lengths of the panels are different and are dependent on their location. The main reason is that the panels that are not located in the center receive lower heat flux; therefore, larger length is required to reach 700℃. Considering Dagget, CA as the location of the power plant, a heliostat field is designed following the approach presented in (Besarati & Goswami 2014). The field parameters are given in Table 2.

Table 2. Field parameters

Heliostats	
Number of heliostats	92
Width	8.84 m
Height	7.34 m
Reflectivity	0.88
Receiver	
Tower height	115 m
Tilt angle of the aperture	35°
Aperture width	3.6 m
Aperture height	2.7 m

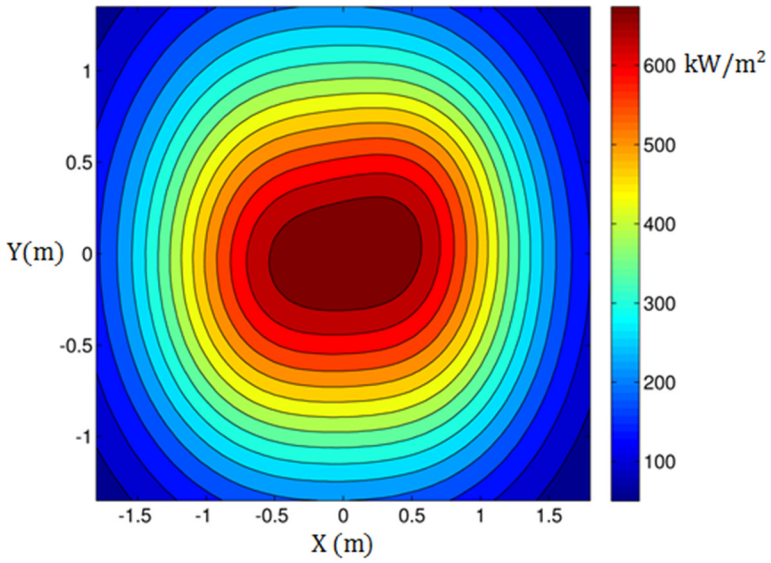

Figure 6. Heat flux density distribution on the receiver surface at noon; March 21st after employing the aiming strategy

Figure 6 demonstrates the heat flux density distribution on the receiver surface at noon; March 21st , after employing the aiming strategy method presented by (Besarati et al. 2014). The maximum heat flux is received in the center, which is close to 700 $\mathrm{kW/m^2}$. On the other hand, the minimum heat flux is received around the corners and is about 50 $\mathrm{kW/m^2}$. That is the reason the panels are not located at the corners of the surface (Figure 5).

Thermal model

There are three types of the surfaces inside the cavity: 1) Active surfaces which receive the direct heat flux and transfer it to s-CO_2 through the CHE. 2) Cornered surfaces which are located at the corners beside the active surfaces. 3) Inactive surfaces which include top, bottom, left and right sides of the cavity. There are two main types of thermal losses, i.e. convective and radiative heat losses.

Convective heat loss

The natural heat transfer coefficient for each surface is determined using the method proposed by (Clausing 1981). The forced heat transfer coefficient is obtained by the correlation proposed by (Siebers & Kraabel 1984). The overall heat transfer coefficient is found by:

$$h_c = h_{nc} + h_{fc} \quad (17)$$

In this study, the ambient temperature is fixed at 35℃. According to the weather data files and correlations, the wind speed is taken as 10 $\frac{\mathrm{m}}{\mathrm{s}}$ at tower height.

Radiative heat loss

Radiative heat loss inside the cavity is simulated using the model presented in (Teichel 2011). The net radiative heat transfer between surface i and surface j is given by:

$$\dot{Q}_{rad,i,j} = \dot{Q}_{rad,thermal,i,j} + \dot{Q}_{rad,solar,i,j} \quad (18)$$

where

$$\dot{Q}_{rad,thermal,i,j} = \varepsilon_{j,therm}\,\varepsilon_{i,therm}\,\sigma\,A_i\,\hat{F}_{i,j,therm}\left(\left(1-f_{0-\lambda_{step},T_i}\right)T_i^4-\left(1-f_{0-\lambda_{step},T_j}\right)T_j^4\right) + \varepsilon_{j,solar}\,\varepsilon_{i,solar}\,A_i\,\hat{F}_{i,j,solar}\left(f_{0-\lambda_{step},T_i}T_i^4-f_{0-\lambda_{step},T_j}T_j^4\right) \quad (19)$$

and

$$\dot{Q}_{rad,solar,i,j} = f_{0-\lambda_{step},T_{sun}}\hat{F}_{i,j,solar}\,A_i\,\varepsilon_{solar,i}\,\varepsilon_{solar,j}\left(Flux_{solar,i}-Flux_{solar,j}\right) + \left(1-f_{0-\lambda_{step},T_{sun}}\right)A_i\,\hat{F}_{i,j,therm}\,\varepsilon_{i,therm}\,\varepsilon_{j,therm}\left(Flux_{solar,j}-Flux_{solar,i}\right) \quad (20)$$

The net radiative heat transfer rate from surface i can be obtained by summing the above equations for all surfaces j. The factor $\hat{F}_{i,j}$ represents the fraction of the total radiation leaving surface i and directly or indirectly falling on surface j (Teichel 2011). In this study, the emissivity of the active surfaces is 0.95 for wavelengths below λ_{step} while it reduces to 0.1 for larger wavelengths. That is the reason there are two different terms for emissivity, i.e. ε_{solar} for short wavelengths and ε_{therm} for larger wavelengths. Moreover, λ_{step} is taken as 3 μm and the emissivity for cornered and inactive surfaces is 0.1.

Energy balance on the surfaces

For the active surfaces:

$$Flux_i\,A_i = Q_{HTF,i} + Q_{conv,loss,i} + Q_{rad,loss,i} \quad (21)$$

For the cornered surfaces:

$$Flux_i\,A_i = 0 + Q_{conv,loss,i} + Q_{rad,loss,i} \quad (22)$$

For the inactive surfaces:

$$0 = 0 + Q_{conv,loss,i} + Q_{rad,loss,i} \quad (23)$$

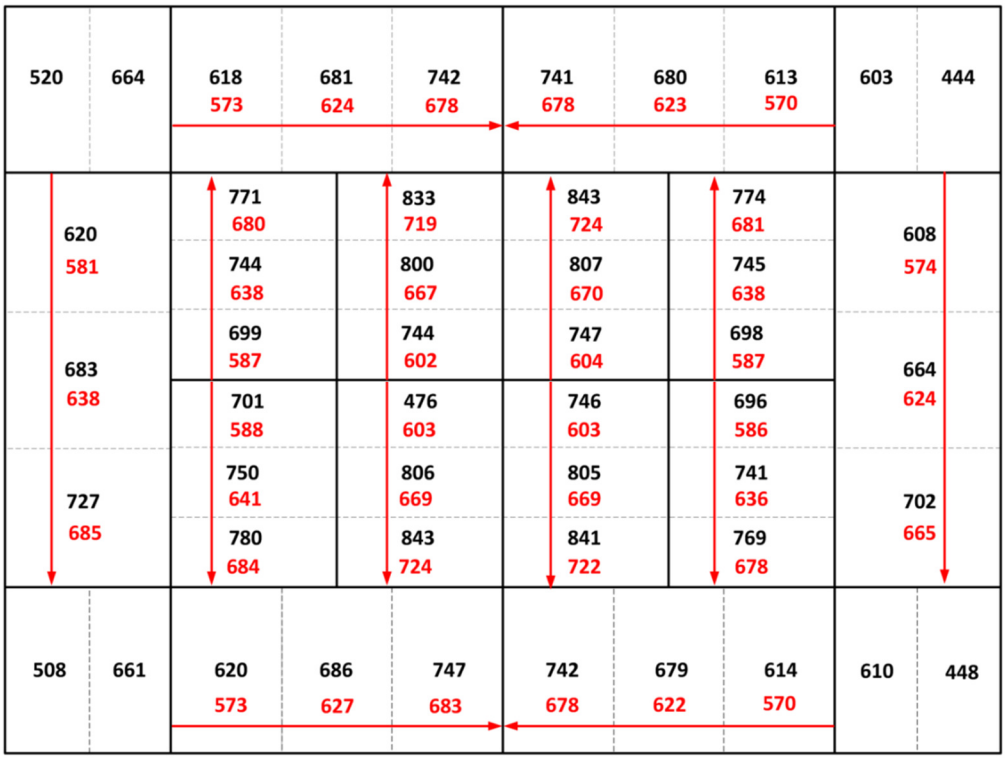

Figure 7. S-CO_2 (red) and surface (black) temperatures

These equations can be solved by iterating the surface temperatures. Each active panel is divided into three surfaces to obtain more accurate temperature profiles. Figure 7 presents the fluid and surface temperatures. Red arrows demonstrate the direction of the fluids inside the CHEs.

The mean s-CO_2 temperature leaving the receiver is 691℃, which is very close to the target value (700℃). The maximum surface temperature is 843 ℃ which is much below the maximum temperature limit of Inconel 625, i.e. 982℃. The receiver efficiency is obtained as:

$$\eta_{rec} = \frac{Q_{transfered\ to\ the\ fluid}}{Q_{received\ by\ the\ receiver}} \times 100 = 81.22\ \%$$

It is noteworthy that such high efficiency is achieved even without optimizing the cavity geometry. The efficiency can be further improved with optimization.

SUMMARY AND CONCLUSIONS

A direct s-CO_2 receiver was designed based on the principles of compact heat exchangers. The heat transfer and pressure drop models were developed and validated against available data in the literature. The receiver is designed to heat s-CO_2 from 530℃ to 700℃. The geometry of the receiver was determined using multi-objective the Pareto based optimization approach by the simultaneous minimization of the unit thermal resistance and the pressure drop. Then, a 3MW_{th} cavity receiver was designed using 14 individual panels. The heliostat field was designed, and the corresponding flux distribution on the receiver surface was obtained for March 21st. Next, the radiative and convective heat transfer models were developed, and the bulk fluid and surface temperatures were obtained. The results showed that the s-CO_2 reached the design temperature while the surface temperatures remained below the maximum temperature limit of Inconel 625. The receiver efficiency was obtained as 81.22%, which is highly promising. However, the efficiency can be further improved by optimizing the geometry of the cavity receiver. Considering the appropriate thermal and mechanical performance of the CHEs, they can be seriously considered for the next generation of high temperature pressurized solar receivers.

NOMENCLATURE

A	area (m^2)
a	channel width (m)
b	channel height (m)
C	loss coefficient
C_p	specific heat $(J/kg/K)$
D_h	hydraulic diameter (m)
E	joint factor
$Flux$	solar heat flux (W/m^2)
$\hat{F}$	F-hat parameter
f	friction factor
$f_{0-\lambda_{step}}$	fraction of radiation emitted with the wavelength below λ_{step}
H	heat exchanger height (m)
h	convective heat transfer coefficient $(W/K/m^2)$
h_c	overall convective heat transfer coefficient inside the cavity $(W/K/m^2)$
h_{nc}	natural convective heat transfer coefficient inside the cavity $(W/K/m^2)$
h_{fc}	forced convective heat transfer coefficient inside the cavity $(W/K/m^2)$
L	heat exchanger length (m)
l_n	unit grid length (m)

m number of layers
$\dot{m}$ mass flow rate (kg/s)
n number of unit grids
$\dot{Q}$ heat transfer (W)
q heat flux (W)
$q^{"}$ heat flux density (W/m^2)
R_{base} base conduction thermal resistance (K/W)
$R_{b,conv}$ base convection thermal resistance (K/W)
$R_{w,conv}$ wall convection thermal resistance (K/W)
R_{cond} axial conduction thermal resistance (K/W)
R_{wall} wall conduction thermal resistance (K/W)
RR unit thermal resistance $(K/W/cm^2)$
S design stress (MPa)
S_m membrane stress (MPa)
S_T total stress (MPa)
$T_{bulk,f}$ bulk fluid temperature (K)
$T_{f,in}$ fluid inlet temperature $K)$
T_j junction temperature (K)
T_s surface temperature (K)
$\overline{T_s}$ average surface temperature (K)
t base thickness (m)
t_p plate thickness (m)
t_f distance between the adjacent channels(m)
V mean fluid velocity (m/s)
W_{hx} heat exchanger width (m)
ΔP pressure drop (kPa)
ρ fluid density (kg/m^3)
α channel aspect ratio
ε_{solar} emissivity in the solar wavelength band
ε_{therm} emissivity in the thermal wavelength band
λ_{step} the wavelength at which the emissivity changes
η_{rec} receiver thermal efficiency

REFERENCES

Anon, 1998, " *ASME Boiler &* Pressure *Vessel Code, Section III* ".

Besarati, S.M. & Goswami, D.Y., 2013, "Analysis of Advanced Supercritical Carbon Dioxide Power Cycles With a Bottoming Cycle for Concentrating Solar Power Applications", *Journal of Solar Energy Engineering*, 136(1), p.011020.

Besarati, S.M. & Goswami, D.Y., 2014, "A computationally efficient method for the design of the heliostat field for solar power tower plant ", *Renewable Energy*, 69, pp.226–232.

Besarati, S.M., Goswami, D. Y. & Stefanakos, E.K., 2014, " Optimal heliostat aiming strategy for uniform distribution of heat flux on the receiver of a solar power tower plant ", *Energy Conversion and Management*, 84, pp.234–243.

Clausing, A. M., 1981, " An analysis of convective losses from cavity solar central receivers ", *Solar Energy*, 27(4), pp.295–300.

Deb, K., Pratap, A., Agarwal, S., & Meyarivan, T., 2002., " A fast and elitist multiobjective genetic algorithm: NSGA-II ", *IEEE Transactions on Evolutionary Computation*, 6(2), pp.182–197.

Dostal, V., 2004, " *A supercritical carbon dioxide cycle for next generation nuclear reactors* ", Massachusetts Institute of Technology (MIT).

Everhart, J.L., 1971. *Engineering properties of nickel and nickel alloys*, PLENUM Press.

Firouzdor, V. et al., 2013. Corrosion of a stainless steel and nickel-based alloys in high temperature supercritical carbon dioxide environment. *Corrosion Science*, 69, pp.281–291.

Gibbs, J.P., 2010, "*Corrosion of various engineering alloys in supercritical carbon dioxide*", Massachusetts Institute of Technology.

Gnielinski, V., 1976, " New equations for heat and mass transfer in turbulent pipe and channel flow.pdf. *International chemical engineering "*, 16(2), pp.359–368.

Hesselgreaves, J.., 2001, " *Compact heat exchangers: Selection, Design and operation*", Access Online via Elsevier.

Idelchik, I.E., 1994, "*Handbook of hydraulic resistance"*, CRC Press.

Lei, N., 2006," *The thermal characteristics of multilayer minichannel heat sinks in single-phase and two-phase flow* ", The University of Arizona.

Lei, N., Ortega, A. & Vaidyanathan, R., 2007," Modeling and optimization of multilayer minichannel heat sinks in single-phase flow ", *ASME InterPACK conference*,Vancouver, British Columbia, pp. 29–43.

Lemmon, E.W., Mclinden, M.O. & Huber, M.L., 2013, "NIST Reference Fluid Thermodynamic and Transport Properties" , NIST standard reference database 23.

Li, Q., Flamant, G., Yuan, X., Neveu, P., & Luo, L., 2011, "Compact heat exchangers: A review and future applications for a new generation of high temperature solar receivers ", *Renewable and Sustainable Energy Reviews*, 15(9), pp.4855–4875.

Pierres, R. Le, Southall, D. & Osborne, S., 2011, " Impact of mechanical design issues on printed circuit heat exchangers ", *SCO2 Power Cycle Symposium*, University of Colorado at Boulder, CO.

Siebers, D.L. & Kraabel, J.S., 1984, " Estimating convective energy losses from solar central receivers ", *Sandia National Laboratories, Livermore, SAND84-8717*.

Teichel, S.H., 2011, " *Modeling and calculation of heat transfer relationships for concentrated solar power receivers*", University of Wisconsin-Madison.

Turchi, C.S., 2009, "Supercritical CO 2 for Application in Concentrating Solar Power Systems ", *Proceedings of SCO2 Power Cycle Symposium*, RPI, Troy, NY, pp. 1–5.

Turchi, C. S., Ma, Z., Neises, T., & Wagner, M., 2012, " Thermodynamic study of advanced supercritical carbon dioxide power cycles for high performance concentrating solar power systems", *Proceedings of the ASME 2012 6th International Conference on Energy Sustainability ES2012*, San Diego, CA, USA.